Flexible Constant-Power Range Extension of Self-Oscillating System for Wireless In-Flight Charging of Drones

Yu Gu, *Member, IEEE*, Jiang Wang, *Member, IEEE*, Zhenyan Liang, *Member, IEEE*, and Zhen Zhang, *Senior Member, IEEE*

***Abstract*—The special challenge for drone wireless in-flight charging is to keep a constant charging power with a large air gap under the variation of mutual inductance and the limited payload of pickup. To solve the issue, this article proposes a flexible constant-power (CP) range extension scheme with the self-oscillating wireless power transfer system, which is achieved on the primary side. By changing the duty cycle, the proposed autonomous ON–OFF keying modulation (AOKM) scheme can effectively expand and regulate the CP region with high flexibility, avoiding the usual pickup-side-only implementation. With the AOKM scheme, the operating frequency is autonomously adjusted to keep the CP output, where only the primary current needs to be sensed without the dc–dc converter or wireless communication. Thus, it ensures the lightweight pickup of drones. The experimental results verify that the transfer distance of the CP region can be extended by 62.4%, while keeping a constant power of 73.8 W and efficiency of 88.3% regardless of the changed air gap and misalignment. Hence, based on the proposed flexible CP range extension (AOKM) scheme, the large-range CP charging region with high efficiency can be obtained for the drone wireless in-flight charging system, thus prolonging the flight time of drones.**

***Index Terms*—Autonomous ON–OFF keying modulation (AOKM), drone, self-oscillating, wireless power transfer.**

I. Introduction

DRONE has been extensively adopted in aerial photography and grid inspection over the past decades [1], [2]. Whereas, the flight time of drone is usually only half an hour due to the limited drone battery capacity, which hardly meets the demand of continuous operations over long times and large regions [3]. To extend the flight time of drones, wireless power transfer (WPT) shows the huge superiority with its electrical isolation, safety, and flexibility [4], [5]. Especially in the special scene (no flat landing site), compared with the landed wireless charging, the wireless in-flight charging is an ideal solution for drones, as shown in Fig. 1. It can theoretically extend flight time to infinity,

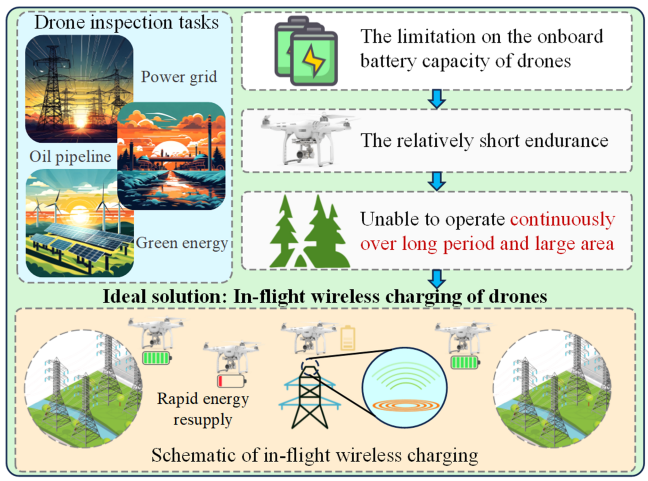

Fig. 1. Schematic diagram of drone wireless in-flight charging.

and ensure fast power supply and uninterrupted operation [6], [7]. Besides, the in-flight drones can perform line monitoring tasks with their long range and wide angle of view during the in-flight charging process. However, different from other WPT applications such as electric vehicle (EV) [8], [9], motor [10], [11], and lighting [12], [13], the drone in-flight charging system faces the special challenge: How to achieve a large-range constant power (CP) charging with high flexibility under the change of mutual inductance (relative position of coils) and the limited payload on the pickup of drones?

For the wireless charging of drones, there are many methods to overcome the mutual inductance disturbance, which mainly consist of coil structure design [14], [15], [16], [17] and various control strategy [18], [19], [20], [21]. In the coil structure design, Cao et al. [14] presented a squirrel-cage receiver coil to enhance misalignment tolerance of WPT system, and an integrated compensation coil has been proposed in [16] to combine with the pickup coil, thus achieving ±150-mm landing deviations for drones. Moreover, in consideration of drone rotational misalignment, Li et al. [17] proposed a magnetic coupler with a vertical square air-core coil to improve the corresponding tolerance. Though the above coil designs can achieve a high misalignment tolerance for landing wireless charging of drones, it may be not enough for the in-flight charging of drones, since a large transfer

Manuscript received 2 February 2024; revised 18 April 2024, 19 May 2024, and 1 July 2024; accepted 5 August 2024. Date of publication 9 August 2024; date of current version 11 September 2024. This work was supported by the National Natural Science Foundation of China under Grant 52377013. Recommended for publication by Associate Editor M. Vitelli. *(Corresponding author: Zhen Zhang.)*

The authors are with the School of Electrical and Information Engineering, Tianjin University, Tianjin 300072, China (e-mail: guyu1997@tju.edu.cn; jiangwang@tju.edu.cn; liangzy@tju.edu.cn; zhangz@tju.edu.cn).

Color versions of one or more figures in this article are available at https://doi.org/10.1109/TPEL.2024.3440963.

Digital Object Identifier 10.1109/TPEL.2024.3440963

distance and a continuously varied mutual inductance will exist in the scenario.

Besides, the control strategies mainly focus on double-side control [18], [19] and single-side control [20], [21]. The online-trained neural network is adopted in [18] to ensure the constant output for the drone in-flight charging, and a dynamic coupling coefficient estimation method is proposed for the application to control to keep high efficiency under the coupling variation [19]. Whereas, the above methods require wireless communication, which is not suitable for the in-flight drone due to possible data losses and increased payload on drones. In addition, a mutual-inductance prediction scheme based on high-order topology is proposed for control [20] by ignoring the internal resistances of coils, which only needs the primary detection. But the control accuracy may be affected when the internal resistance is large.

Apart from the above control schemes, the self-oscillating control strategy has attracted the attention of researchers with its merits of high efficiency while keeping the constant output [22], [23]. In the self-oscillating WPT system, the autonomous frequency adjustment can be achieved to keep the CP charging in the strong coupling region, which is practical for drone in-flight charging. Whereas, when the transfer distance is large, namely in the weak coupling of the WPT system, the charging power will still be affected by the changed relative position between coupling coils. Therefore, it is necessary to expand and adjust the CP region, namely realizing a larger transfer distance, which can meet the application demands of various situations.

To expand the transfer distance of WPT system, traditional methods include parameter optimization [23], repeater coil [24], and magnetic materials [25]. By increasing the self-inductance of pickup coil, the CP region of the self-oscillating system can be extended with the reduction of critical coupling [23]. But due to space and weight constraints, the self-inductance of pickup coil cannot be indefinitely enlarged. In addition, when system parameters are fixed, the CP region cannot be adjusted to the desired value. The repeater resonator is proved in [24] to extend the transfer distance, but the coupling strength from repeater to the transmitting and pickup coils are needed to be identical, which is hard to realize in the drone wireless charging. Besides, while nanocrystalline material and ferrites facilitate coupling strength [25], the consequent increased weight and magnetic loss should be considered along with the extended distance.

It's worth noting that in distinction to other WPT applications, the in-flight charging of drones face the challenges of the large transfer distance, continuous changes of mutual inductance and the limited payload. First, the transfer distance between the in-flight drone and transmitting coil is large for the safety purpose. Meanwhile, the continuous disturbance of mutual inductance is caused by variations of air gap and misalignment between the coupling coils, which should be overcome to keep a large-range CP charging for drone. In addition, the extra weight on the pickup side of drones will increase the energy loss when the drone is hovering and prolong the charging time, hence the excessive weight increase on the pickup side should be avoided. Finally, for various types of drones and different application scenes, the flexible CP range extension with minimum weight on pickup side is needed to achieve. Hence, a large-range CP charging with high flexibility is necessary under the above challenges of drone wireless in-flight charging system.

Accordingly, to overcome the above challenges, this article proposes a novel flexible CP range extension scheme based on the self-oscillating system for in-flight charging of drone, which has the salient advantages of the long-range robustness, high flexibility and pickup lightweight. Compared with other self-oscillating systems [22], [23], by using the proposed primary-side modulation, transfer distance and misalignment tolerance of CP output can be expanded and flexibly adjusted, avoiding the situation that is usually realized only on the pickup side. In short, the contributions of the proposed method are listed as follows.

1) The autonomous ON–OFF keying modulation (AOKM) is proposed to realize the CP range extension of self-oscillating WPT system with the reduction of critical coupling coefficient, thus meeting the demand for a wide-range charging application against the mutual inductance disturbance.
2) The flexible extension of the CP range can be obtained by changing duty cycle of the AOKM on the primary side without any extra topology or hardware on the pickup, which shows the salient features of convenience and high system flexibility.
3) The whole control circuit for the CP range extension with autonomous frequency regulation is achieved on the primary side. Thus, the extra payload on drones is avoided to reduce the power loss of in-flight drones and prolong the flight time.

II. Theoretical Analysis and Modeling

A. Coupled Modeling of the Self-Oscillating WPT System

The circuit diagram of the proposed self-oscillating WPT system for the drone wireless in-flight charging is shown in Fig. 2(a), which mainly includes the inverter, transmitter, pickup, rectifier, and load. S_1–S_4 constitute a full-bridge inverter, which can converter the dc voltage $V_{\rm dc}$ to high frequency ac voltage u_p. Here, L_p, L_s, and M_{ps} are the self-inductances of the transmitting and pickup coils and mutual inductance between them. C_p and C_s are compensation capacitors. R_p and R_s are the internal resistances of transmitter and pickup, respectively. R_{eq} is the equivalent resistance of drone battery R_{dro} after rectification. To achieve the CP region extension, inverter switching signals with the proposed AOKM can be shown in Fig. 2(b), which will be introduced in Section II-B. Meanwhile, the proposed scheme can also be applied in other topologies, such as the S/PS topology [23].

In the self-oscillating WPT system, the input voltage (u_p) is controlled to be in opposite phase of the input current ($-i_p$). Then, dc source with inverter can be equivalent to a negative resistor ($-R_N$), as shown in Fig. 3(a). Besides, the phasor diagram of the voltages and currents of transmitter and pickup can be shown in Fig. 3(b). With the control circuit, the operating frequency will autonomously change with the variation of coupling coefficient, thus achieving the constant output features, which has the great superiority. However, the CP range is required to be flexibly expanded due to the limitations of practical applications.

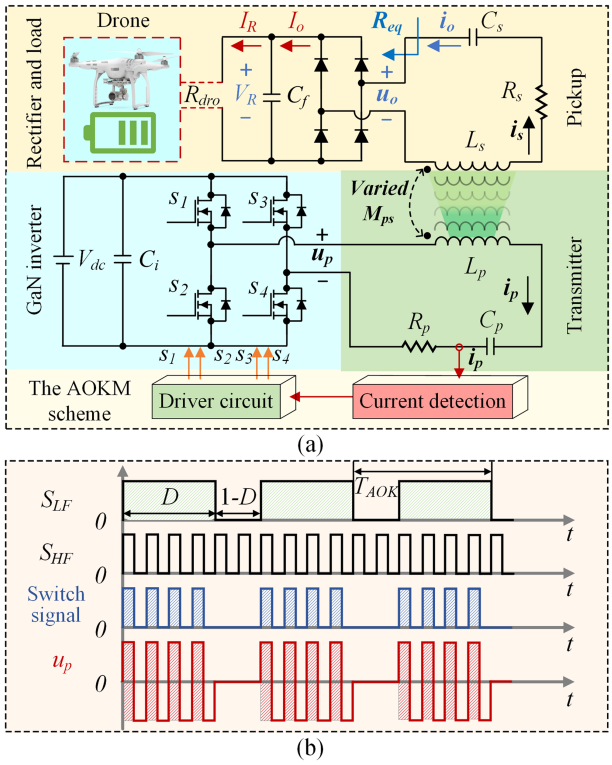

Fig. 2. (a) System diagram. (b) Switching signals for inverter.

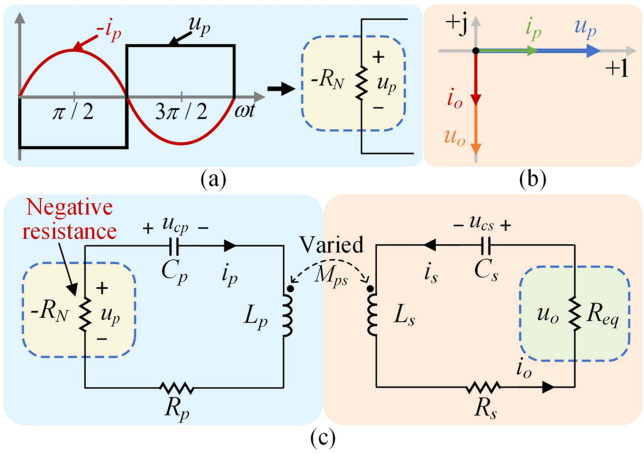

Fig. 3. (a) Inverter output voltage and current. (b) Phasor diagram for current and voltage. (c) Equivalent circuit of the self-oscillating system.

To facilitate the analysis of energy transmission between the coupled resonators, the coupled-mode theory (CMT) model of the self-oscillating WPT system is adopted. Fig. 3(c) shows the equivalent circuit model, where i_p, i_s, and i_o denote the currents flowing through L_p, L_s, and R_{eq}, respectively. u_{cp} and u_{cs} are the voltages of C_p and C_s. Based on Fig. 3(c), the circuit equations of the self-oscillating WPT system can be expressed as

$$\begin{cases} L_p\frac{di_p}{dt}+M_{ps}\frac{di_s}{dt}+u_{cp}+i_pR_p=u_p \\ M_{ps}\frac{di_p}{dt}+L_s\frac{di_s}{dt}+u_{cs}+i_s\left(R_s+R_{eq}\right)=0 \\ C_p\frac{du_{cp}}{dt}=i_p \\ C_s\frac{du_{cs}}{dt}=i_s. \end{cases} \tag{1}$$

Based on the fundamental harmonics approximation method, the inverter voltage u_p satisfies that $u_p=4V_{\rm dc}/(\sqrt{2}\pi)$. According to the CMT model, the energy modes ψ_p and ψ_s of the transmitting and pickup resonators can be described as

$$\begin{cases} \psi_p=\Psi_p e^{j(\omega t+\theta_p)}=\sqrt{\frac{L_p}{2}}i_p+j\sqrt{\frac{C_p}{2}}u_{cp} \\ \psi_s=\Psi_s e^{j(\omega t+\theta_s)}=\sqrt{\frac{L_s}{2}}i_s+j\sqrt{\frac{C_s}{2}}u_{cs} \end{cases} \tag{2}$$

where ω is the system operating frequency, Ψ_p, Ψ_s and θ_p, θ_s are the amplitudes and phases of the energy modes, respectively. Based on (1) and (2), the circuit state variables of the self-oscillating system can be expressed in the energy model as

$$\begin{cases} i_p=\Psi_p\sqrt{\frac{2}{L_p}}\cos\left(\omega t+\theta_p\right) \\ u_{cp}=\Psi_p\sqrt{\frac{2}{C_p}}\sin\left(\omega t+\theta_p\right) \\ i_s=\Psi_s\sqrt{\frac{2}{L_s}}\cos\left(\omega t+\theta_s\right) \\ u_{cs}=\Psi_s\sqrt{\frac{2}{C_s}}\sin\left(\omega t+\theta_s\right). \end{cases} \tag{3}$$

Besides, the natural resonant frequencies of transmitting and pickup resonators are denoted as $\omega_p=1/\sqrt{L_pC_p}$ and $\omega_s=1/\sqrt{L_sC_s}$. For the self-oscillating WPT system, it should satisfy $\omega_p=\omega_s=\omega_0$. Based on the averaging method [26], it is assumed that the amplitudes and phases of the energy modes are constant, and the high-frequency terms can be eliminated. Then, substituting (2) and (3) into (1), the dynamic equations can be derived as

$$\frac{d}{dt}\begin{bmatrix}\psi_p\\ \psi_s\end{bmatrix}=\begin{bmatrix} j\omega_0+\frac{1}{\Psi_p}\frac{2V_{\rm dc}}{\pi\sqrt{2L_p}}-\frac{R_p}{2L_p} & -j\kappa\frac{\omega_0}{2} \\ -j\kappa\frac{\omega_0}{2} & j\omega_0-\frac{R_s+R_{eq}}{2L_s}\end{bmatrix}\begin{bmatrix}\psi_p\\ \psi_s\end{bmatrix} \tag{4}$$

where $\kappa=M_{ps}/\sqrt{L_pL_s}$ is the coupling coefficient between the transmitting and pickup coils. According to (4), the frequency characteristic equation of the proposed system can be obtained

$$\begin{vmatrix} j\left(\omega_0-\omega\right)+\frac{1}{\Psi_p}\frac{2V_{\rm dc}}{\pi\sqrt{2L_p}}-\frac{R_p}{2L_p} & -j\kappa\frac{\omega_0}{2} \\ -j\kappa\frac{\omega_0}{2} & j\left(\omega_0-\omega\right)-\frac{R_s+R_{eq}}{2L_s}\end{vmatrix}=0. \tag{5}$$

With the separation of the real and imaginary parts of (5), it can be expressed as (6), and the steady solution of the operation frequency ω is derived as (7)

$$\begin{cases} \frac{\kappa^2\omega_0^2}{4}-\left(\omega-\omega_0\right)^2+\left(\frac{R_p}{2L_p}-\frac{1}{\Psi_p}\frac{2V_{\rm dc}}{\pi\sqrt{2L_p}}\right)\left(\frac{R_s+R_{eq}}{2L_s}\right)=0 \\ \left(\omega-\omega_0\right)\left(\frac{1}{\Psi_p}\frac{2V_{\rm dc}}{\pi\sqrt{2L_p}}-\frac{R_p}{2L_p}-\frac{R_s+R_{eq}}{2L_s}\right)=0 \end{cases} \tag{6}$$

$$\omega=\begin{cases}\omega_0\pm\sqrt{\left(\frac{\kappa\omega_0}{2}\right)^2-\left(\frac{R_s+R_{eq}}{2L_s}\right)^2}=\omega_{1,2}, & \kappa\geq\kappa_c \\ \omega_0, & \kappa<\kappa_c\end{cases} \tag{7}$$

Thus, the operation frequency ω will stabilize at different values with the changed coupling coefficient. Here, the critical

coupling coefficient κ_c is expressed as (8), which is pivotal for the extension and regulation of the CP region

$$\kappa_c = \frac{R_s + R_{eq}}{\omega_0 L_s}. \tag{8}$$

Significantly, when natural resonant frequency ω_0 is fixed, the critical coupling κ_c is mainly dependent on the parameters of the pickup. The value of κ_c can be reduced with a large self-inductance L_s or a small equivalent load R_{eq} (R_s can be ignored with respect to R_{eq}). Based on (8), there are two steady operation regions for the self-oscillating WPT system, namely the strong coupling region ($\kappa \geq \kappa_c$) and the weak coupling region ($\kappa < \kappa_c$).

In the strong coupling region, based on (7), the system operating frequency will autonomously stabilize at $\omega_{1,2}$ rather than ω_0 [22], which will change with the coupling coefficient κ. And, the amplitudes of the energy modes can be expressed as

$$\Psi_p = \Psi_s = \frac{2\sqrt{2L_p}L_s V_{\text{dc}}}{\pi\left[R_p L_s + (R_s + R_{eq})\, L_p\right]}. \tag{9}$$

By substituting (9) to (3), the current ratio can be deduced

$$\left|\frac{i_p}{i_s}\right| = \sqrt{\frac{L_s}{L_p}}. \tag{10}$$

It can be found that i_s is in fixed proportion to i_p. By detecting primary current, the output current can be estimated, which can help to regulate the output power against the other disturbance, such as load. Meanwhile, the output power P_{out} and efficiency η of the self-oscillating WPT system can be obtained as

$$P_{\text{out}} = \frac{R_{eq}\Psi_s^2}{L_s} = \frac{8V_{\text{dc}}^2 R_{eq} L_p L_s}{\pi^2\left[R_p L_s + (R_s + R_{eq})\, L_p\right]^2} \tag{11}$$

$$\eta = \frac{R_o \Psi_s^2 / L_s}{R_p \Psi_p^2 / L_p + (R_s + R_{eq})\, \Psi_s^2 / L_s} = \frac{R_{eq}}{R_p\,(L_s/L_p) + R_s + R_{eq}}. \tag{12}$$

It can be observed from (11) and (12) that the output power and efficiency of the self-oscillating system are independent of coupling coefficient κ in the strong coupling region, which has outstanding superiority for the drone charging. But it is worth noting that the CP range can be obtained only when κ is larger than κ_c. The smaller the value of κ_c, the larger the CP range. Thus, to obtain a large range of CP region for application, it is necessary to reduce and regulate κ_c to the desired smaller value.

In the weak coupling region, the system operating frequency will stabilize at ω_0. Based on (6) and (7), the amplitudes of the energy modes Ψ_p and Ψ_s can be expressed as

$$\Psi_p = \frac{2\sqrt{2L_p}V_{\text{dc}}\,(R_s + R_{eq})}{\pi\left[\kappa^2\omega_0^2 L_p L_s + (R_s + R_{eq})\, R_p\right]} \tag{13}$$

$$\Psi_s = \frac{2\sqrt{2L_p}L_s\omega_0 V_{\text{dc}}}{\pi\left[\kappa^2\omega_0^2 L_p L_s + (R_s + R_{eq})\, R_p\right]}. \tag{14}$$

Besides, the output power and efficiency can be expressed as (15) and (16), which are the identical to the magnetic resonant coupling WPT system

$$P_{\text{out}} = \frac{8V_{\text{dc}}^2 R_{eq}\omega_0^2\kappa^2 L_p L_s}{\pi^2\left[\omega_0^2\kappa^2 L_p L_s + R_p\,(R_s + R_{eq})\right]^2} \tag{15}$$

$$\eta = \frac{R_{eq}\omega_0^2\kappa^2 L_p L_s}{\omega_0^2\kappa^2 L_p L_s\,(R_s + R_{eq}) + R_p(R_s + R_{eq})^2}. \tag{16}$$

It is obvious that the output power and efficiency still change with coupling coefficient when $\kappa < \kappa_c$, which should be avoided for the constant output. To obtain a large-range CP region, the value of κ_c should be reduced. Based on (8), the CP region of the self-oscillating WPT system will be extended with a large pickup coil L_s or a small equivalent load R_{eq}. But due to space and weight constraints, L_s cannot be increased indefinitely. With the high-order topology, a small equivalent load can be obtained to expand the CP region. Whereas, this will increase the power losses of in-flight drones with the resulting additional weight. Besides, κ_c will be nonadjustable with fixed parameter, which is not conducive to the flexible regulation of the desired CP region for various drones and different application scenarios. Therefore, to obtain the CP output with a large transfer distance, the key challenge for the in-flight charging of drones is: *How to achieve the expansion and regulation of the CP region of the self-oscillating system by using only the primary modulation?*

B. Autonomous On–Off Keying Modulation

To solve the challenge mentioned above, this article presents a novel AOKM scheme on primary side to expand and regulate the CP region of the self-oscillating WPT system, thus avoiding the problem that can usually be realized only on the pickup side. In fact, the traditional ON–OFF keying (OOK) modulation is mainly applied to regulate the equivalent load of WPT system to achieve the maximum transfer efficiency [27], [28], while a soft-start scheme has been proposed to solve the problem of high surge currents [29]. Compared with the traditional OOK, the proposed AOKM aims to achieve a flexible expansion of the CP region of the WPT system with the primary side control, which can ensure a stable output under a wide range of coupling coefficient fluctuations. Here, the constant charging power can be obtained with the autonomous regulation of operating frequency. Meanwhile, by changing duty cycle D online, the CP region can be expanded and regulated with the proposed AOKM. The whole control circuit is on the primary side without any dc–dc converter on the pickup, which is suitable for the lightweight design of in-flight charging of drones. The specific description is as follows.

The principle of the AOKM scheme for the self-oscillating system is the regulation of the duty cycle D for the inverter on the primary side, thus adjusting the equivalent load R_{eq} of the pickup. Based on (8), the critical coupling κ_c will be reduced with the decreased equivalent load R_{eq} by reducing the duty cycle online. Then, the CP region is expanded. Meanwhile, with the change of mutual inductance, the operating frequency of the AOKM scheme will autonomously adjust to keep the CP output.

Fig. 2(b) shows the switching signals for the inverter based on the proposed AOKM scheme. It can be seen that the high-frequency signal S_{HF} and low-frequency signal S_{LF} are given to control the inverter. Here, the frequency of S_{HF} is autonomously regulated to keep the CP based on (7), and S_{LF} contains n pulses of S_{HF}, where n is usually large. It is worth noting that the switch signal will be logic-high only when S_{HF} and S_{LF} are both logic-high. Here, D represents the duty cycle of the AOKM scheme, and T_{AOK} is the control period. Then, the inverter will cycle through the active and idle states in turn, respectively.

As shown in Fig. 2(a), in the active state, I_o is denoted as the average output current of the diode rectifier on the load side. And, the current of drone battery and the load voltage are I_R and V_R, where $R_{dro} = V_R/I_R$. In a period of T_{AOK} time, the output energy of the rectifier should be equal to the received energy of drone battery, which can be expressed as

$$E_o = V_R I_o D T_{AOK} = V_R I_R T_{AOK}. \tag{17}$$

Here, the diode rectifier bridge is adopted on the pickup side. Thus, in the pickup side, the relationship between the amplitude of fundamental component U_{o1} of the pickup output voltage u_o and the load voltage V_R satisfies

$$U_{o1} = \frac{4V_R}{\pi}. \tag{18}$$

When ignoring the power loss of the diode rectifier bridge, the input power of the diode rectifier bridge should be equal to the power flowing out the diode rectifier. Hence, based on the above definition of equivalent load R_{eq}, the output power P_{out} of the self-oscillating WPT system can be expressed as

$$P_{\mathrm{out}} = \frac{U_{o1}^2}{2R_{eq}} = V_R I_o. \tag{19}$$

Then, by substituting (17) and (18) into (19), the equivalent load R_{eq} of the self-oscillating WPT system with the proposed AOKM scheme can be derived as

$$R_{eq} = \frac{8V_R^2}{\pi^2 V_R I_o} = D\frac{8}{\pi^2}\frac{V_R}{I_R} = D\frac{8}{\pi^2}R_{dro}. \tag{20}$$

Then, according to (8), (11) and (12), the critical coupling κ_c, efficiency η and output power P_{out} of the self-oscillating WPT system with the AOKM scheme can be re-expressed as

$$\kappa_c = \frac{R_s + 8DR_{dro}/\pi^2}{\omega_0 L_s} \tag{21}$$

$$P_o = DP_{\mathrm{out}} = \frac{64D^2V_{\mathrm{dc}}^2 L_p L_s R_{dro}/\pi^2}{\pi^2\left[R_p L_s + \left(R_s + 8DR_{dro}/\pi^2\right)L_p\right]^2} \tag{22}$$

$$\eta = \frac{8DR_{dro}/\pi^2}{R_p\left(L_s/L_p\right) + R_s + 8DR_{dro}/\pi^2}. \tag{23}$$

It is worth noting that based on (21), the critical coupling κ_c will be reduced with a small value of the duty cycle D, hence expanding the CP range of the self-oscillating system. By changing D on the primary side, the robust charging range can be flexibly regulated with the extra degree of freedom and high flexibility. Based on (22) and (23), it can be observed that the output power and efficiency are still independent of mutual inductance within a larger CP range. Accordingly, by applying the proposed AOKM scheme on the primary side, the CP range extension and regulation can be achieved without any extra weight on the pickup, hence effectively improving the system stability and adaptability for the drone in-flight charging.

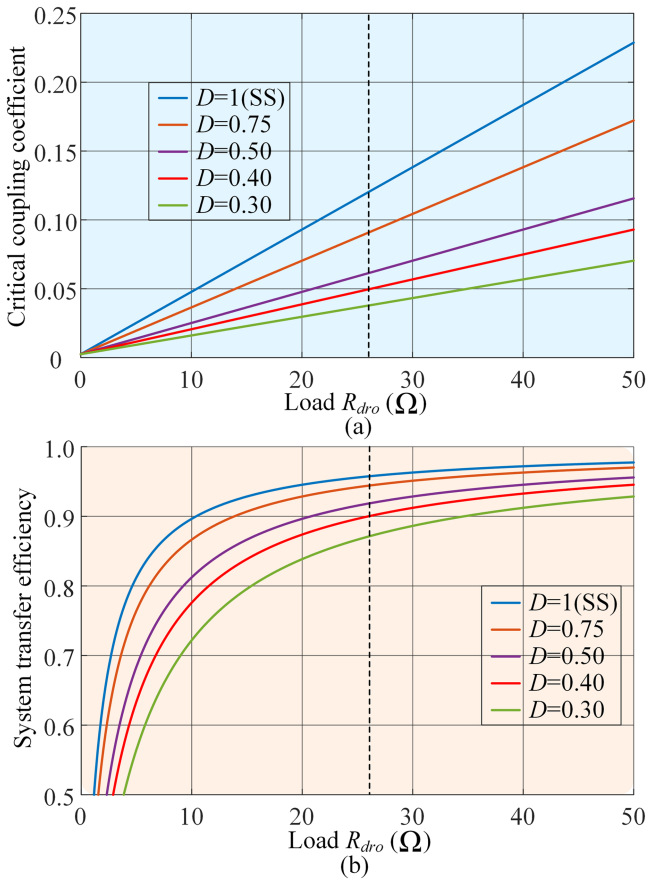

Fig. 4. Curves of (a) critical coupling coefficient κ_c and (b) transfer efficiency η versus load R_L with different duty cycles D.

III. System Implementation

A. Transmission Characteristics

Based on the theoretical analysis, the output characteristics of the self-oscillating system with the proposed AOKM scheme can be obtained. According to (21) and (23), it can be manifest that the critical coupling κ_c and efficiency η are mainly related to load R_{dro} and duty cycle D with the fixed parameters. The corresponding curves at different R_{dro} and D are depicted in Fig. 4. It is observed that with a smaller R_{dro}, the critical coupling coefficient κ_c can be greatly reduced, thus effectively expanding the CP region. But the smaller R_{dro} will lead to the decreased transfer efficiency at the same time. To balance the two indicators, a load value of 26 Ω is selected in the article to further analyze the transmission characteristics.

To highlight the flexible extension capacity of the CP region with the proposed AOKM scheme, the output characteristics under different duty cycles D are shown in Fig. 5. Here, yellow area represents the strong coupling region without AOKM and

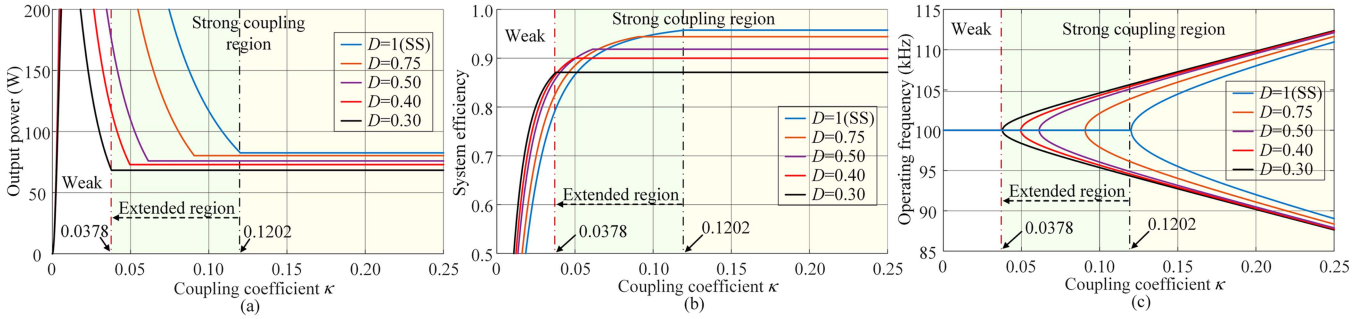

Fig. 5. Transfer characteristic curves with different duty cycles D. (a) Output power versus coupling coefficient. (b) Transfer efficiency versus coupling coefficient. (c) Operating frequency versus coupling coefficient.

green area is the extended CP region with duty cycle of 0.3. It can be observed that the critical coupling is reduced from 0.1202 to 0.0378 by regulating D of the AOKM scheme, hence effectively expanding the CP region. Besides, although there is a small change in output power and efficiency with different D, they are still constant with the change of mutual inductance. Besides, it can be seen from Fig. 5(c) that operating frequency will autonomously stabilize at $\omega_{1,2}$ based on (7). As observed from Fig. 5(b), a smaller D of the AOKM scheme can expand the transfer distance, but it also reduces the transfer efficiency. Accordingly, the appropriate value of D should be selected and regulated to meet the demand of a large-range CP region for various drones and different scenarios, and the efficiency needs to keep as high as possible. It is worth noting that the duty cycle D can be flexibly regulated in a primary-side controller to meet demand of the expanded CP range. Meanwhile, the proposed AOKM does not need complex circuits or additional hardware, and avoids the problem that the CP region extension can usually be realized only on the pickup side. Thus, it has great advantage of convenience and flexibility for the drone in-flight charging.

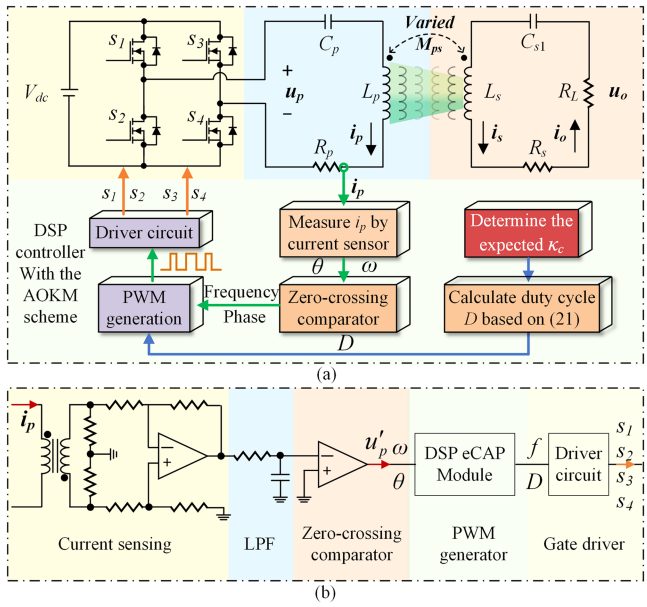

Fig. 6. Block diagram of (a) self-oscillating WPT system with the proposed AOKM scheme. (b) Signal processing circuit of controller.

B. Control With the Proposed AOKM Scheme

Fig. 6 shows the block diagram of the self-oscillating WPT system with the proposed AOKM scheme for the flexible CP range extension. The AOKM scheme includes the autonomous frequency regulation and the ON–OFF keying modulation. Based on the analysis in Section II, autonomous frequency regulation can be obtained when the phase difference of equivalent voltage and current flowing through it is kept 180°, as shown in Fig. 3. Here, the phase synchronization method (PSM) based on digital signal processing (DSP) controller is applied to realize the autonomous frequency regulation. As shown in Fig. 6(a), the phase θ and frequency ω of the primary current i_p are sensed with the detection circuit, which are sent to the DSP controller with the generation of the complementary inverter switching signals. Then, the output voltage of inverter up is generated, with its phase 180° from i_p. With the autonomous frequency regulation, the CP range against mutual inductance can be obtained in the strong coupling region based on (22). Besides, after determining the expected κ_c, the duty cycle can be adjusted to expand the CP region with high flexibility. It is worth noting that the whole control circuit of the proposed AOKM scheme is on the primary side without dc–dc converter on the pickup, which is suitable for the lightweight design of in-flight charging of drones.

The detailed AOKM scheme of the controller is shown in Fig. 6(b). The primary current i_p is first detected by current sensor, and a square wave u'_p in phase with i_p is generated by passing through the low-pass filter and zero-crossing comparator. Then, the rising edge of u'_p is recognized by the eCAP module of DSP, which includes the phase and period information of i_p. Hence, the high-frequency signal S_{HF} can be generated in the DSP. By controlling low-frequency signal S_{LF}, which contains n pulses of S_{HF}, duty cycle D of the AOKM scheme in a period T_{AOK} can be regulated. With the selection of duty cycle, low-frequency signal S_{LF} is also generated. Finally, the switch signal based on S_{LF} and S_{HF} is sent to the gate driver of inverter, which can ensure the phase difference between i_p and u_p. Hereby, the operation frequency of the WPT system will autonomously stabilize at $\omega_{1,2}$ with the change of the mutual inductance in the strong coupling region. Based on (21), the critical coupling coefficient κ_c will reduce with the decreased of duty cycle D. Accordingly, with the proposed AOKM scheme, the flexible CP region extension

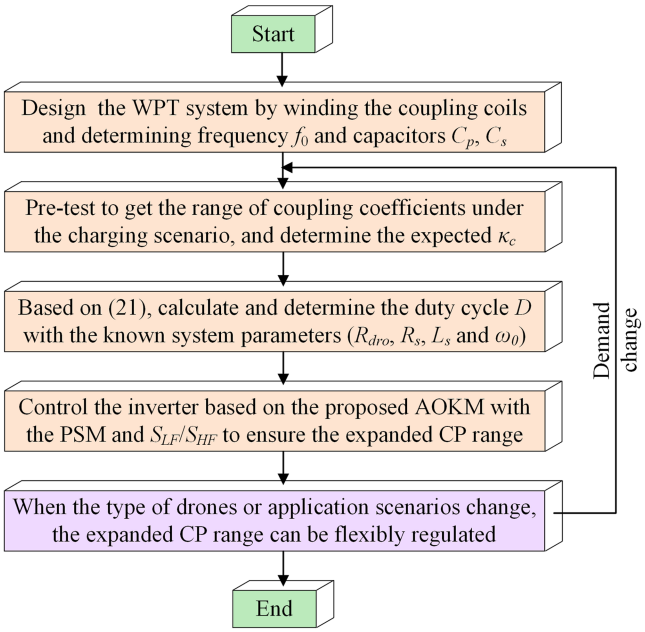

Fig. 7. Control flowchart for the flexible CP range extension.

for the self-oscillating system can be achieved with the extra degree of freedom D.

The control flowchart of the proposed AOKM scheme is presented in Fig. 7. First, the parameters of the coupling coil are determined based on the structure of the drone, including the inner and outer diameters. Then, the self-inductance of coupling coil and mutual inductance under the desired transfer distance are calculated using the precise modelling equations of coils [30], [31]. Simulation software can also be used to verify the theoretical values. Then, according to the charging scenario and the type of drone, the experimental pretest can be operated to get the range of coupling coefficients for the drone in-flight charging region. To obtain the constant charging power, the minimum coupling coefficient in the pretest can be taken as the expected value of κ_c. Then, with the known system parameters, the duty cycle D can be determined to get the expected κ_c based on (21). It is worth noting that though κ_c can be further reduced, to ensure high efficiency, the expected κ_c is just enough to ensure the CP range. Finally, based on the PSM, autonomous frequency regulation with duty cycle D can be applied to obtain the expanded CP region. Besides, when the expected CP range is necessary to be adjusted or expanded due to the new application scenario, there is no need to add new hardware circuits or adjust the circuit parameters, only the duty cycle needs to be changed for the new scenario, which shows high flexibility and convenience for the actual application.

Moreover, it should be mentioned that the realization of the proposed AOKM scheme is different from the traditional pulse density modulation (PDM). To generate the switch signal of the traditional PDM, the switching time and frequency are fixed and known in advance. While generating the switch signal of AOKM, the primary current is first transformed into a square wave u_p, which is then captured by the eCAP to get its phase and period. And the switch signal will autonomously change its frequency based on the capture of eCAP. Hence, the AOKM needs to accurately capture the phase and period information to regulate the frequency with the system clock of DSP. Here, the software phase compensation is adopted to compensate for the time delay of hardware circuit. Besides, the AOKM involves both analog signal processing and digital signal processing. Meanwhile, the self-oscillating WPT system can be easily and reliably controlled to operate at ω_1 or ω_2. As long as the value of period register PRD in the DSP is limited to be less or greater than PRD_0 ($\mathrm{PRD}_0 = 2\pi/(\omega_0 \mathrm{T_{CLK}})$, And $\mathrm{T_{CLK}}$ is the time required for the counter to increment by 1). Here, low frequency ω_2 is selected as the operating frequency, which can reduce the switching and conduction loss of inverter switching devices.

In conclusion, based on the proposed AOKM scheme, the expanded region for the constant charging power is kept against the change of mutual inductance with high flexibility. Besides, compared with the usual pickup-side-only implementations for the CP region extension, the whole detection and control unit of AOKM is set up on the primary side, which avoids the extra payload on drones, hence extending the in-flight time of drones.

TABLE I
KEY PARAMETERS OF PROTOTYPE

Parameters	Symbol	Value
Inductance of transmitting coil	L_p	140.7 μH
Capacitance of primary side	C_p	18.02 nF
Resistance of primary side	R_p	0.24 Ω
Inductance of pickup coil	L_s	285.1 μH
Capacitance of series capacitor	C_s	8.89 nF
Resistance of secondary side	R_s	0.45 Ω
Resistance of load	R_L	26 Ω
Distance between coils	d	60–165 mm
System natural operating frequency	f_0	100 kHz
Period of the AOKM scheme	T_{AOK}	200/f
Capacitance of DC capacitor	C_f	680 μF

IV. SIMULATION

To verify the validity of the proposed flexible CP range extension method, the simulation model of the self-oscillating WPT system is built by MATLAB/Simulink with the parameter, as listed in Table I. By considering the transfer performance and electromagnetic radiation, the natural resonant frequency is designed to be 100 kHz. Meanwhile, other common frequencies of the WPT system can also be applied for the proposed AOKM scheme. For different expected values of κ_c, the simulated duty cycle D under various loads R_{dro} can be shown in Fig. 8. Here, curves and triangles (squares) in different colors represent the theoretical and simulation values. Based on (21), duty cycle requires to be lower for the expected smaller value of κ_c. It is clearly observed that duty cycle at different R_{dro} can be adjusted to track the expected κ_c with the proposed AOKM, thus ensuring the flexible CP range extension. In addition, the simulated values of D agree well with the theoretical values.

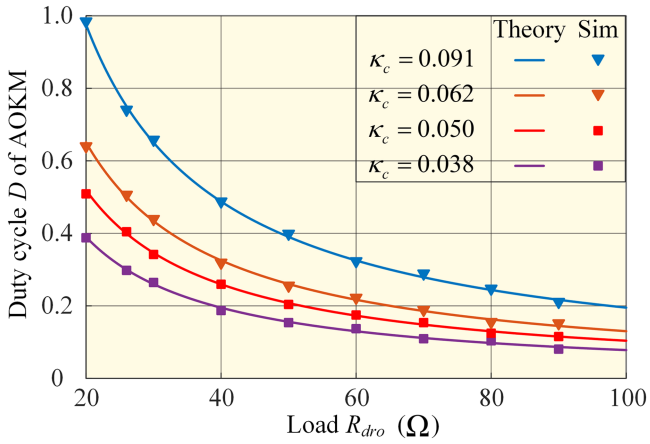

Fig. 8. Duty cycle D of the AOKM versus loads R_{dro} at different critical coupling coefficients κ_c (0.091, 0.062, 0.050, and 0.038).

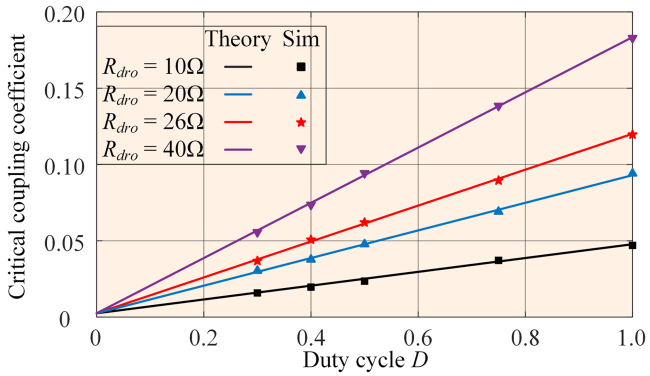

Fig. 9. Critical coupling coefficient κ_c with different duty cycles D of the AOKM scheme at different loads R_L (10 Ω, 20 Ω, 26 Ω, and 40 Ω).

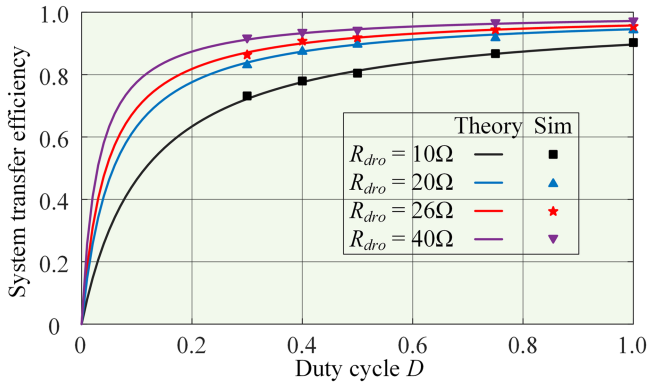

Fig. 10. Transmission efficiency with different duty cycles D of the AOKM scheme at different loads R_L (10 Ω, 20 Ω, 26 Ω, and 40 Ω).

Moreover, to compare the output characteristics at different duty cycles D, the critical coupling coefficient and efficiency of the proposed system are shown in Figs. 9 and 10. It can be seen that the critical coupling κ_c at different loads will be decreased with the reduction of D, and the efficiency will decrease at the same time. It shows that the simulated results well verify theoretical analysis. When $R_{dro} = 26\ \Omega$, to expand the CP region with a high efficiency, D can be selected as 0.4,

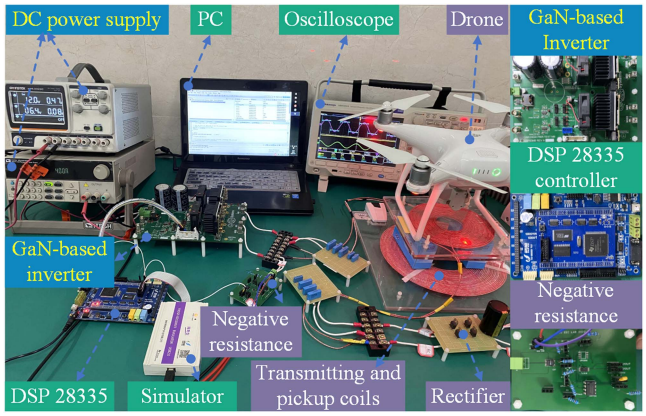

Fig. 11. Experimental prototype.

where κ_c is reduced from 0.1202 to 0.0495 with the efficiency of 90.2%. Accordingly, the proposed AOKM scheme of the self-oscillating WPT system can easily expand the CP range for the drone wireless in-flight charging to satisfy the requirements of long-range charging.

V. Experiment

A. Experimental Results of the Proposed System

To verify the feasibility of the proposed flexible CP region extension method, the prototype with the parameters as listed in Table I is constructed for experimentation. As shown in Fig. 11, the proposed system includes power source (Itech IT6722A), GaN-based inverter (GSP65R13HB-EVB), signal processing circuit, WPT circuit topology, DSP controller, rectifier bridge, and load. The coupling coils are made of the tightly wound Litz wire (Φ: 0.1 mm × 200 strands) and no magnetic material has been added. It is worth noting that though magnetic materials such as ferrite can increase the coupling strength and, thus, expand the CP region, their increased size and weight need to be taken into account due to the limitation of installation space. Besides, especially in the strong coupling region, when the relative position between coupling coils changes, the increase of magnetic materials will affect the self-inductance of coupling coils. Whereas the frequency detuning caused by the change in self-inductance will not ensure constant output features in the proposed WPT system. The polypropylene capacitors are adopted as compensation capacitors, and the Schottky rectifier (STPS20120D) with low forward voltage drop is used to form the rectifier bridge. The experimental waveforms are analyzed and displayed on the oscilloscope (MDO3024).

To realize the proposed AOKM scheme of self-oscillating WPT system, the detection and control circuits are designed, as shown in Fig. 6(b). The primary current is sampled by the current transformer (CU8965) with the turns ratio of 1:100. And the current signal is further amplified and converted into the voltage signal by a differential sampling circuit consisting of a high-speed operational amplifier (LM6172). Then, the zero-crossing detection circuit composed of a high-speed comparator (TL3016) is used to identify the zero-crossing point of primary-side current, and the corresponding in-phase signal is captured

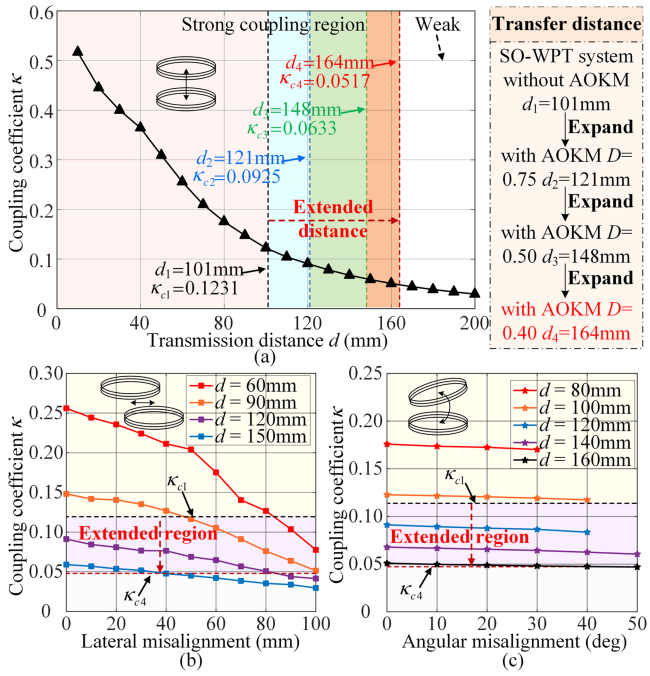

Fig. 12. Experimental results of the coupling coefficient κ between the coils (a) versus transfer distances; (b) versus lateral misalignments; (c) versus angular misalignments with different transfer distances.

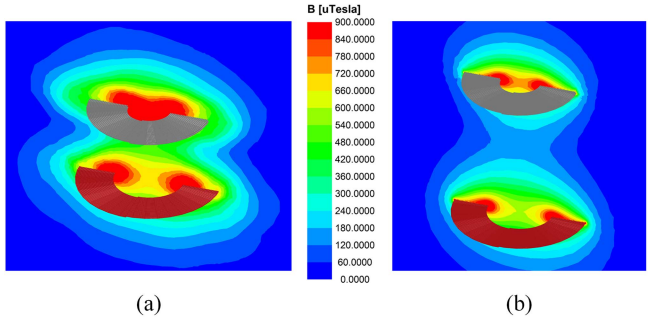

Fig. 13. Magnetic field distribution of the coupling coils adopted in the proposed system (a) transfer distance $d = 90$ mm; (a) $d = 180$ mm.

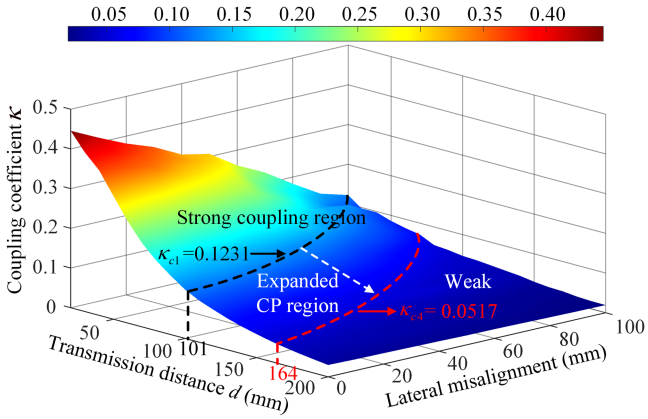

Fig. 14. Experimental results of the coupling coefficient κ at different transmission distances and lateral misalignments.

by the eCAP module of DSP controller (TMS320F28335) to obtain the phase and operating frequency. With the desired duty cycle, the proposed AOKM scheme is implemented on the DSP and generates drive signals, which is used to control the inverter by the driver Si8271. The inverter output voltage and current are kept in the inverse phase to achieve the proposed self-oscillating system, namely the negative resistance. Hence, the automatic frequency adjustment is realized under the change of coupling coefficients to ensure that the output is nearly constant.

The measured coupling coefficients κ at different transfer distances are shown in Fig. 12(a). It can be observed that the maximum transfer distance of CP region is 101 mm without the AOKM scheme. With the regulation of duty cycle, the critical coupling coefficient κ_c has been reduced, thus expanding the transfer distance of the CP region. Significantly, the transfer distance can be extended to 164 mm at $D = 0.4$ with an expansion of 62.4%. Meanwhile, considering that both lateral and angular misalignments between the coupling coils may happen in drone in-flight charging system. To verify the misalignment tolerance features of the proposed AOKM scheme, the measured values of κ at different distances and misalignments are shown in Fig. 12(b) and (c), where κ_{c1} and κ_{c4} are the critical coupling with $D = 1$ and 0.4, respectively. It can be seen that by regulating the duty cycle from 1 to 0.4, the higher misalignment tolerance (both lateral and angular misalignments) of the self-oscillating WPT system is achieved with the reduction of κ_c from 0.1231 to 0.0517, which agrees well with the theoretical analysis result. Meanwhile, the finite element analysis of the proposed coupling mechanism is carried out by using MAXWELL. Fig. 13 shows the magnetic field distribution at different transfer distances (90 mm and 180 mm), where 90 mm and 180 mm are in the strong coupling and weak coupling region, respectively.

In addition, to more intuitively see the expanded CP region under different transfer distances and lateral misalignments, Fig. 14 displays the corresponding three-dimensional diagram of the coupling coefficient κ, which can cover the common range for the drone in-flight charging. The black dashed line and the red dashed line are the critical coupling coefficients of the self-oscillating WPT system without and with the proposed AOKM, respectively. It can be clearly observed that the CP range of the self-oscillating system has been effectively expanded with the duty cycle of 0.4. Accordingly, the experimental results validate the practicality of the proposed flexible CP range expansion method, which is suitable for the long-range wireless charging of in-flight drones.

To compare the output features with different duty cycles of the AOKM, Figs. 15–18 show the experimental waveforms of the proposed self-oscillating WPT system at different transfer distances in four cases ($D = 0.4$, 0.5, 0.75, and 1). It can be noted that the output voltage and current of the inverter are in phase, i.e., a negative resistance can always be obtained. Meanwhile, based on (21)–(23), the CP region can be flexibly expanded by changing duty cycle with the reduction of critical coupling κ_c, whose theoretical output features can be found from Fig. 5. As shown in Fig. 15, the experimental waveforms with $D = 1$ indicate that the output power can be kept constant at 83 W with

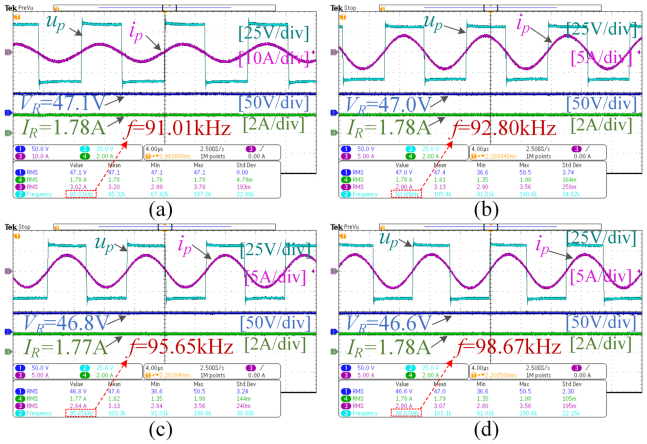

Fig. 15. Experimental waveforms of the self-oscillating WPT system without the proposed AOKM scheme (namely with $D = 1$) at different distances d. (a) $d = 60$ mm. (b) $d = 75$ mm. (c) $d = 90$ mm. (d) $d = 100$ mm.

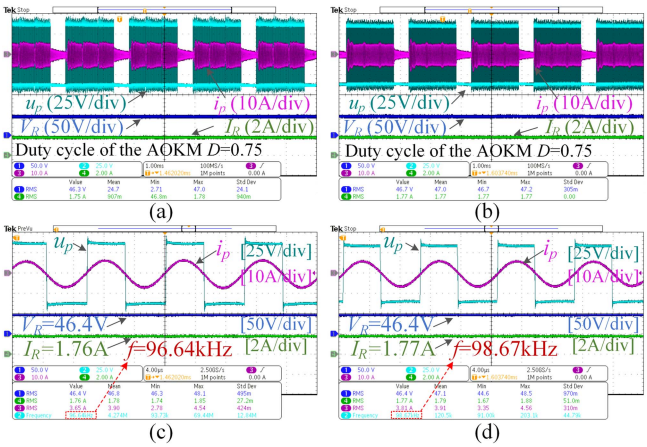

Fig. 16. Experimental waveforms of the self-oscillating WPT system with $D = 0.75$ at different distances d. (a) $d = 100$ mm. (b) $d = 120$ mm. (c) $d = 100$ mm after zooming in. (d) $d = 120$ mm after zooming in.

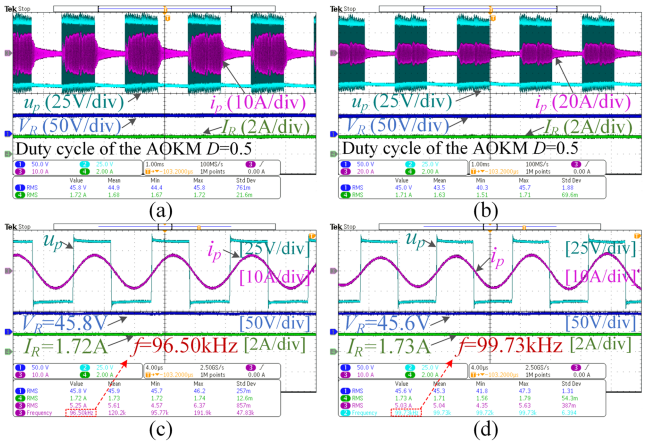

Fig. 17. Experimental waveforms of the self-oscillating WPT system with $D = 0.5$ at different distances d. (a) $d = 120$ mm. (b) $d = 150$ mm. (c) $d = 120$ mm after zooming in. (d) $d = 150$ mm after zooming in.

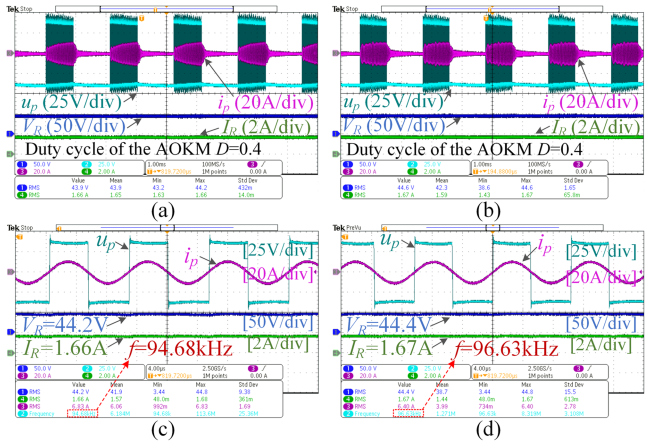

Fig. 18. Experimental waveforms of the self-oscillating WPT system with $D = 0.4$ at different distances d. (a) $d = 100$ mm. (b) $d = 120$ mm. (c) $d = 100$ mm after zooming in. (d) $d = 120$ mm after zooming in.

different distances d (60, 75, 90, and 100 mm). However, when the distance $d > 101$ mm, namely in the weak coupling region, the output power will vary with the changed transfer distance or misalignment, which shows the limitations of the conventional self-oscillating WPT system. Hence, the CP range of the system is required to be expanded with the proposed AOKM scheme. As shown in Fig. 12(a) above, the maximum distances of the CP region can be adjusted and extended to about 121 mm, 148 mm, and 164 mm with $D = 0.75$, 0.5, and 0.4, respectively. It verifies the proposed AOKM scheme has the ability to flexibly adjust the CP region extension. Meanwhile, Fig. 16 shows the waveforms with $D = 0.75$ at the distances $d = 100$ mm and 120 mm.

It can be seen that the output current and voltage are almost constant at different distances with the automatically changed frequency. Thus, its output power in the strong coupling region is constant at 81.8 W against the transfer distance. Besides, the experimental waveforms with $D = 0.5$ at the distances $d = 120$ mm and 150 mm are shown in Fig. 17, and the waveforms with $D = 0.4$ at the distances $d = 100$ mm and 120 mm are also shown in Fig. 18. The experimental results validate that the proposed AOKM scheme can expand the CP region of the self-oscillating WPT system with high flexibility and robustness.

In addition, to demonstrate the state variables of the pickup circuit in the proposed system, the voltage and current before and after rectification are shown in Fig. 19. It can be observed that the voltage u_o is almost a square wave with 50% duty cycle and the waveform of i_s is sinusoidal at different duty cycles, thus, the diode rectifier operates in continuous current mode, which verifies the accuracy of (18). Therefore, (20)–(23) can be considered correct. Meanwhile, the start-up process of the proposed system at different duty cycles ($D = 0.4$ and 1) is shown in Fig. 20. It can be seen that the average regulation time of start-up process is about 130 ms, which can meet the demand of drone in-flight charging application. More importantly, the system can ensure the constant power charging demand even if the drone attitude fluctuates after the start-up of system. It is worth noting that during start-up, the circuit has a large surge

TABLE II
COMPARATIVE ANALYSIS BETWEEN THE PROPOSED SYSTEM AND OTHERS

Ref.	Scheme	Misalignment tolerance /distance expansion ratio	High system flexibility	Meet pickup lightweight?	No wireless communication?	Output power (W)	Transfer efficiency	Frequency (MHz)	Distance (cm)	Size of Tx / Rx (cm)
[14]	Magnetic coupler	Tolerance: 50%	Unexpected	Yes	Yes	135.8	80%	0.085	--	44×44/4×20
[16]	Magnetic coupler	Tolerance: 54%	Unexpected	Yes	Yes	150	80.6%	0.15	5.0	56×56/16×16
[17]	Magnetic coupler	Rotation: 360°	Good	Yes	Yes	113.6	88.6%	0.5	--	50×50/10×20
[18]	Control method	Expansion: 50%	Unexpected	No	No	25	--	0.1	7.5	20×20/14×14
[20]	Control method	Expansion: 37%	Unexpected	Yes	Yes	20	82.1%	0.1	8.0	20×20/14×14
[32]	Magnetic coupler	Tolerance: 37%	Good	No	No	126	91.6%	0.085	8.0	40×40/20×20
[34]	Control method	Not mention	Unexpected	Yes	Yes	10	93.6%	1	10.0	26×26/14×14
This paper	Control method	Expansion: 62.4%	Good	Yes	Yes	73.8	88.3%	0.1	16.4	30×30/20×20

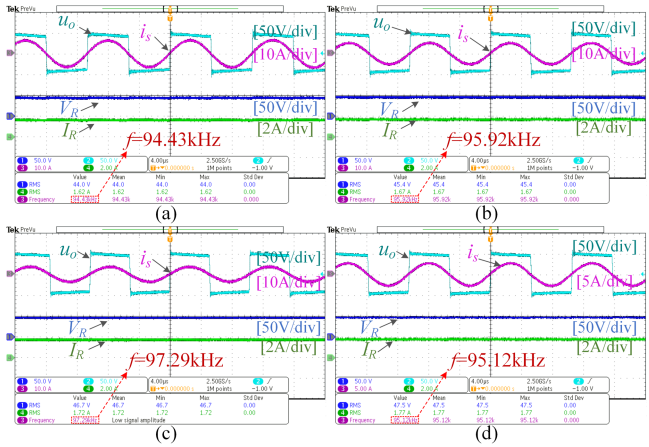

Fig. 19. Experimental waveforms of i_s, u_o, V_R, and I_R in the self-oscillating WPT system. (a) $D = 0.4$. (b) $D = 0.5$. (c) $D = 0.75$. (d) $D = 1$.

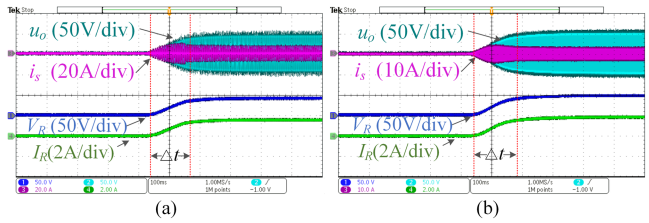

Fig. 20. Startup state of the proposed system. (a) $D = 0.4$. (b) $D = 1$.

current due to the nature of high-Q resonant circuit. A soft-start scheme has been proposed in [29] to suppress the overcurrent current, however, it will reduce the transmission efficiency of the WPT system. The main focus of this article is on the flexible expansion of the constant power region of the self-oscillating WPT system, so the issue of current overshoot is not included.

Furthermore, the output performances (operating frequency, output power, and transfer efficiency) of the proposed system for different transfer distances with $D = 0.4$, $D = 0.75$, and $D = 1$ are depicted in Fig. 21. It can be found that the experimental results of the proposed system are close to the theoretical analysis. The differences in the experimental results are mainly due to the additional losses in the switching devices in the actual system, which are not considered in the theoretical derivation. Based on theoretical analysis in Section II, the self-oscillating WPT system can be autonomously stabilized at $\omega_{1,2}$ in the strong coupling region. From Fig. 21(a), it can be observed that the experimental operating frequencies f of the proposed system are basically consistent with the theoretical value $\omega_{1,2}$ based on (7). Meanwhile, when the coils are aligned with the transfer distance of less than 164 mm, a constant output power at about 73.8 W can be achieved with the transfer efficiency of 88.3% regardless of the changed transfer distance. Besides, as shown in Fig. 21, the blue area is the strong coupling region without the AOKM, and the red area is the expanded CP region with $D = 0.4$ using the AOKM scheme. It can be observed that the maximum transfer distance has been expanded from 101 mm to 164 mm. Meanwhile, by regulating duty cycle D, the CP region can be further adjusted and extended. Accordingly, with the proposed AOKM scheme, the large-range constant charging output of the self-oscillating WPT system can be obtained with high flexibility and lightweight for the drone in-flight charging, which can overcome the disturbance of mutual inductance.

Besides, the power loss analysis of the proposed system for the cases ($D = 0.4$, 0.5, 0.75, and 1) is given here. As shown in Fig. 22, the power loss of the system mainly includes the coil loss, inverter loss, and rectifier loss. With the duty cycle $D = 1$, the efficiency is 91.7%, and the total loss is 7.5 W. When $D = 0.4$, the efficiency is 88.3%, and the total loss is 9.8 W. Though the efficiency decreases with $D = 0.4$, the decrease is not more than 4%. More importantly, the transfer distance with $D = 0.4$ can be increased by 62.4% relative to the system without the AOKM scheme, showing great advantages. Moreover, the proposed CP region extension does not need complex circuit topology or any extra hardware. Meanwhile, the detection and control circuits are on the primary side without dc–dc converter and wireless communication, which can improve the real-time and guarantee the lightweight design of drones. Accordingly, the proposed AOKM scheme based on the self-oscillating WPT system has the competitive advantages for the drone in-flight charging.

B. Comparison With Other Drone Wireless Charging Systems

To highlight the advantages of the proposed self-oscillating WPT system with the AOKM scheme, Table II concludes the comparison of the characteristics and performance parameters between this work and the previous drone charging systems. Particularly, the outstanding advantage of the proposed system is the flexible expansion of the CP charging region with high misalignment tolerance, high system flexibility, and no wireless communication, which avoids the conventional

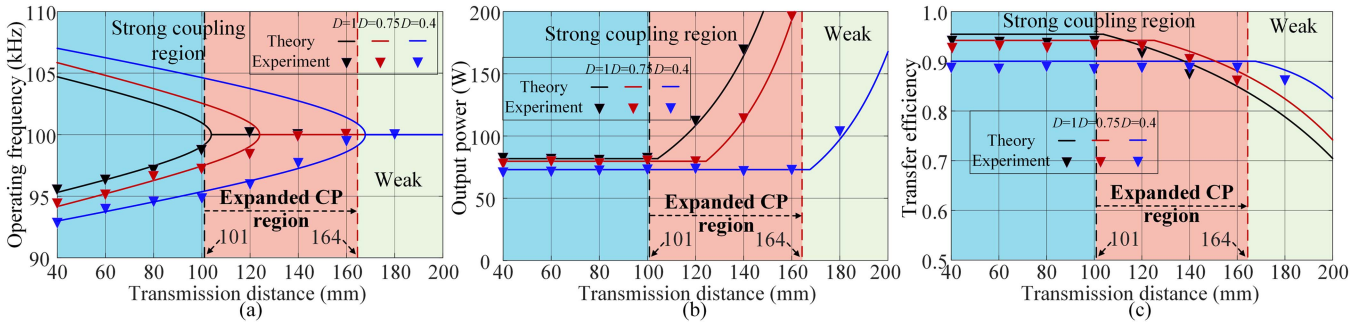

Fig. 21. Theoretical and experimental results of the self-oscillating WPT system with different D. (a) Operating frequency with different transfer distances d. (b) Charging power with different transfer distances d. (c) Transfer efficiency with different transfer distances d.

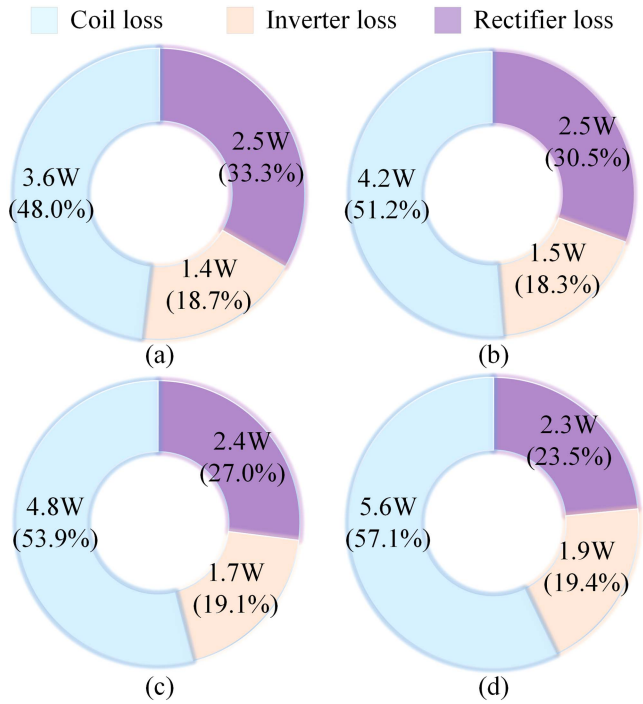

Fig. 22. Power losses analysis of the self-oscillating WPT system with different duty cycles. (a) $D = 1$. (b) $D = 0.75$. (c) $D = 0.5$. (d) $D = 0.4$.

approach to add topology or control circuit on the pickup side and is especially suitable for drone wireless in-flight charging system.

In general, the methods to overcome the mutual inductance variations for drone wireless charging mainly include magnetic coupler design and various control methods. Magnetic coupler design methods normally involve the design of a compact and lightweight coupling coil structure to obtain a uniform magnetic field distribution, thereby improving the system's robustness against mutual inductance change [14], [15], [16], [17], [32]. Whereas, due to the limited improvement in antimutual inductance capability, they are more suitable for drone landed charging at relatively short transfer distances to conquer the impact of landing deviation on the output features. Compared with [14], [15], [16], and [17], the proposed system in the article achieves a large CP region expansion while ensuring high efficiency, which is appropriate for drone in-flight charging. Besides, in the control scheme, a neural network-based control strategy [18] and a primary-side mutual inductance prediction method [20] have been proposed to achieve constant-current output for drone in-flight charging. In contrast to these schemes, the system proposed in this article has higher flexibility to adjust and expand the robust charging range by controlling the duty cycle of the AOKM scheme.

Furthermore, compared with other self-oscillating WPT systems [23], [33], [34], the proposed system in this article adopts the PSM based on DSP to achieve the autonomous frequency regulation, and the proposed AOKM scheme achieves the expansion and regulation of the CP region without adding any topology on the pickup side, hence satisfying various charging demands over large ranges and long distances. Meanwhile, the operating frequency can be chosen to be low frequency to reduce the power losses. A comparison of the specific performance parameters is shown in Table II. It can be seen that the transfer distance of CP region in this article can reach up to 164 mm, which achieves a greater expansion compared to other works. Therefore, the system proposed in this article has the competitive advantages of a larger CP region and high flexibility for drone in-flight charging.

VI. Conclusion

In this article, a novel flexible CP range extension method is proposed to expand the CP region of the self-oscillating WPT system. For the drone in-flight charging system, the particular challenge is to keep constant charging power under the changed mutual inductance, large transfer distance, and limited payload of pickup. With the proposed AOKM scheme, the CP region expansion and regulation can be easily realized on the primary side, avoiding many usual pickup-side-only implementations. In addition, the detection and control circuit are on the primary side without communication link and dc–dc converter, which can improve the system real-time and reduce the drone payload. According to simulated and experimental results, the maximum charging distance of the proposed system can be prolonged by 62.4% with $D = 0.4$, while keeping the constant power of 73.8 W and efficiency of 88.3%. Thus, the long-range CP charging can be ensured for in-flight drones, which enhances the robustness and flexibility of drone wireless in-flight charging system.

REFERENCES

[1] C. Rong et al., "Critical review of recent development of wireless power transfer technology for unmanned aerial vehicles," *IEEE Access*, vol. 11, pp. 132982–133003, 2023.

[2] C. Cai, J. Wang, F. Zhang, X. Liu, P. Zhang, and Y. G. Zhou, "A multichannel wireless UAV charging system with compact receivers for improving transmission stability and capacity," *IEEE Syst. J.*, vol. 16, no. 1, pp. 997–1008, Mar. 2021.

[3] K. Chen and Z. Zhang, "In-flight wireless charging: A promising application-oriented charging technique for drones," *IEEE Ind. Electron. Mag.*, vol. 18, no. 1, pp. 6–16, Mar. 2024.

[4] Y. Liu, C. Liu, Z. Dong, S. Liu, and W. Wang, "A novel wireless energy router for home energy management with omnidirectional power transmission," *IEEE Trans. Ind. Electron.*, vol. 70, no. 9, pp. 8979–8990, Sep. 2023.

[5] H. Pang, F. Xu, W. Liu, C. K. Tse, and K. T. Chau, "Impedance buffer-based reactance cancellation method for CLC-S compensated wireless power transfer," *IEEE Trans. Ind. Electron.*, vol. 71, no. 7, pp. 6894–6906, Jul. 2024.

[6] Y. Gu, J. Wang, Z. Liang, and Z. Zhang, "Communication-free power control algorithm for drone wireless in-flight charging under dual-disturbance of mutual inductance and load," *IEEE Trans. Ind. Inform.*, vol. 20, no. 3, pp. 3703–3714, Mar. 2024.

[7] K. Chen and Z. Zhang, "Rotating-coordinate-based mutual inductance estimation for drone in-flight wireless charging systems," *IEEE Trans. Power Electron.*, vol. 38, no. 9, pp. 11685–11693, Sep. 2023.

[8] P. Zhang, M. Saeedifard, O. C. Onar, Q. Yang, and C. Cai, "A field enhancement integration design featuring misalignment tolerance for wireless EV charging using LCL topology," *IEEE Trans. Power Electron.*, vol. 36, no. 4, pp. 3852–3867, Apr. 2021.

[9] Y. Wang et al., "A misalignment-tolerant hybrid coupler for electric vehicle IPT charging systems," *IEEE Trans. Veh. Technol.*, vol. 72, no. 10, pp. 12845–12856, Oct. 2023.

[10] C. Jiang, K. T. Chau, C. H. T. Lee, W. Han, W. Liu, and W. H. Lam, "A wireless servo motor drive with bidirectional motion capability," *IEEE Trans. Power Electron.*, vol. 34, no. 12, pp. 12001–12010, Dec. 2019.

[11] Z. Xue, K. T. Chau, W. Liu, and Z. Hua, "Magnetic-free wireless self-direct drive motor system for biomedical applications with high-robustness," *IEEE Trans. Power Electron.*, vol. 39, no. 2, pp. 2882–2891, Feb. 2024.

[12] X. Qu, W. Zhang, S.-C. Wong, and C. K. Tse, "Design of a current-source-output inductive power transfer LED lighting system," *IEEE J. Emerg. Sel. Topics Power Electron.*, vol. 3, no. 1, pp. 306–314, Mar. 2015.

[13] W. Liu, K. T. Chau, C. H. T. Lee, C. Jiang, W. Han, and W. H. Lam, "A wireless dimmable lighting system using variable-power variable-frequency control," *IEEE Trans. Ind. Electron.*, vol. 67, no. 10, pp. 8392–8404, Oct. 2020.

[14] P. Cao et al., "Embedded lightweight squirrel-cage receiver coil for drone misalignment-tolerant wireless charging," *IEEE Trans. Power Electron.*, vol. 38, no. 3, pp. 2884–2888, Mar. 2023.

[15] S. Pang, J. Xu, Z. Xie, J. Lu, H. Li, and X. Li, "Lightweight UAV's wireless power transfer system for constant current charging without secondary feedback control," *IEEE Trans. Veh. Technol.*, vol. 72, no. 12, pp. 15611–15621, Dec. 2023.

[16] J. Wang, R. Chen, C. Cai, J. Zhang, and C. Wang, "An onboard magnetic integration-based WPT system for UAV misalignment-tolerant charging with constant current output," *IEEE Trans. Transp. Electrific.*, vol. 9, no. 1, pp. 1973–1984, Mar. 2023.

[17] Y. Li et al., "A new magnetic coupler with high rotational misalignment tolerance for unmanned aerial vehicles wireless charging," *IEEE Trans. Power Electron.*, vol. 37, no. 11, pp. 12986–12991, Nov. 2022.

[18] Z. Zhang, S. Shen, Z. Liang, S. H. K. Eder, and R. Kennel, "Dynamic-balancing robust current control for wireless drone-in-flight charging," *IEEE Trans. Power Electron.*, vol. 37, no. 3, pp. 3626–3635, Mar. 2022.

[19] X. Dai, X. Li, Y. Li, and A. P. Hu, "Maximum efficiency tracking for wireless power transfer systems with dynamic coupling coefficient estimation," *IEEE Trans. Power Electron.*, vol. 33, no. 6, pp. 5005–5015, Jun. 2018.

[20] Y. Gu, J. Wang, Z. Liang, and Z. Zhang, "Mutual-inductance-dynamic-predicted constant current control of LCC-P compensation network for drone wireless in-flight charging," *IEEE Trans. Ind. Electron.*, vol. 69, no. 12, pp. 12710–12719, Dec. 2022.

[21] W. Liu, K. T. Chau, C. H. T. Lee, W. Han, X. Tian, and W. H. Lam, "Full-range soft-switching pulse frequency modulated wireless power transfer," *IEEE Trans. Power Electron.*, vol. 35, no. 6, pp. 6533–6547, Jun. 2020.

[22] S. Assawaworrarit, X. Yu, and S. Fan, "Robust wireless power transfer using a nonlinear parity-time-symmetric circuit," *Nature*, vol. 546, no. 7658, pp. 387–390, Jun. 2017.

[23] Z. Wei, B. Zhang, S. Lin, and C. Wang, "A self-oscillating WPT system with high misalignment tolerance," *IEEE Trans. Power Electron.*, vol. 39, no. 1, pp. 1870–1887, Jan. 2024.

[24] X. Hou, H. Hu, Y. Su, Z. Liu, Z. Deng, and R. Deng, "A multirelay wireless power transfer system with double-sided LCC compensation network for online monitoring equipment," *IEEE J. Emerg. Sel. Topics Power Electron.*, vol. 11, no. 1, pp. 1262–1271, Feb. 2023.

[25] Y. Wang, C. Q. Jiang, C. Chen, T. Ma, X. Li, and T. Long, "Hybrid nanocrystalline ribbon core and flake ribbon for high-power inductive power transfer applications," *IEEE Trans. Power Electron.*, vol. 39, no. 1, pp. 1898–1911, Jan. 2024.

[26] J. A. Sanders, F. Verhulst, and J. A. Murdock, *Averaging Methods in Nonlinear Dynamical Systems*, 2nd ed. Berlin, Germany: Springer-Verlag, 2007.

[27] W. Zhong and S. Y. R. Hui, "Maximum energy efficiency operation of series-series resonant wireless power transfer systems using on-off keying modulation," *IEEE Trans. Power Electron.*, vol. 33, no. 4, pp. 3595–3603, Apr. 2018.

[28] Z. Hua, K. T. Chau, W. Han, W. Liu, and T. W. Ching, "Output controllable efficiency-optimized wireless power transfer using hybrid modulation," *IEEE Trans. Ind. Electron.*, vol. 69, no. 5, pp. 4627–4636, May 2022.

[29] W. Zhong, H. Li, R. Hui, and D. M. Xu, "Current overshoot suppression of wireless power transfer systems with on-off keying modulation," *IEEE Trans. Power Electron.*, vol. 36, no. 3, pp. 2676–2684, Mar. 2021.

[30] S. Liu, J. Su, J. Lai, J. Zhang, and H. Xu, "Precise modeling of mutual inductance for planar spiral coils in wireless power transfer and its application," *IEEE Trans. Power Electron.*, vol. 36, no. 9, pp. 9876–9885, Sep. 2021.

[31] T. Chen, B. Liu, Y. Luo, and Y. Zhang, *Inductance Calculation Manual*. Beijing, China: Machinery Ind. Press, 1992.

[32] Z. Li, J. He, Y. Huo, M. Ban, Y. Liu, and J. Liu, "High-misalignment tolerance and output adjustable wireless charging system via detuned series-series compensated reconfigurable transmission channels," *IEEE Trans. Power Electron.*, vol. 38, no. 10, pp. 11786–11801, Oct. 2023.

[33] Y. Gu, J. Wang, Z. Liang, and Z. Zhang, "A wireless in-flight charging range extended PT-WPT system using S/single-inductor-double-capacitor compensation network for drones," *IEEE Trans. Power Electron.*, vol. 38, no. 10, pp. 11847–11858, Oct. 2023.

[34] J. Zhou, B. Zhang, W. Xiao, D. Qiu, and Y. Chen, "Nonlinear parity-time-symmetric model for constant efficiency wireless power transfer: Application to a drone-in-flight wireless charging platform," *IEEE Trans. Ind. Electron.*, vol. 66, no. 5, pp. 4097–4107, May 2019.

Yu Gu (Member, IEEE) was born in Shanxi, China, in 1997. He received the B.Eng. degree in automation and the Ph.D. degree in control science and engineering from Tianjin University, Tianjin, China, in 2018 and 2024, respectively.

He is a Postdoctoral Fellow with Tianjin University. His current research interests include wireless power transfer and power electronic control.

Jiang Wang (Member, IEEE) received the B.Eng., M.Eng., and Ph.D. degrees in electrical engineering from Tianjin University, Tianjin, China, in 1986, 1989, and 1996, respectively.

He is currently a Full Professor with Tianjin University. He has authored 4 books and 200 peer-reviewed papers. His research interests include nonlinear control, brain-inspired computing, deep learning, data mining, and industrial control.

Zhenyan Liang (Member, IEEE) received the B.Eng. degree in thermal energy and power engineering from Shanghai Jiao Tong University, Shanghai, China, in 2004, and M.S. degree in control science and engineering in 2019 from Tianjin University, Tianjin, China, where she is currently working toward the Ph.D. degree in control science and engineering.

Her current research interests include wireless power transfer and predictive control for electrical drives.

Zhen Zhang (Senior Member, IEEE) received the B.Eng. and M.Eng. degrees in automation from Tianjin University, Tianjin, China, in 2004 and 2007, respectively, and the Ph.D. degree in electrical engineering from The University of Hong Kong, Hong Kong, in 2014.

In 2014, he was a Visiting Scholar with IBM Research Laboratory supported by IBM Global Great Minds Program. Then, he was a Postdoctoral Fellow with The University of Hong Kong. He is currently a Professor of Electrical Engineering with the School of Electrical and Information Engineering, Tianjin University, and an Honorary Associate Professor with the Department of Electrical and Electronic Engineering, The University of Hong Kong. He has authored and coauthored more than 60 internationally refereed papers as well as two books published by Wiley-IEEE Press and Cambridge University Press, respectively. His research interests include advanced control for power conversion with emphasis on wireless power transfer and motor drives.

Prof. Zhang is currently the Chair of IEEE Beijing Section IES Chapter and an Associate Editor for IEEE TRANSACTIONS ON INDUSTRIAL ELECTRONICS, IEEE TRANSACTIONS ON INDUSTRIAL INFORMATICS, and IEEE Industrial Electronics Magazine. He is the recipient of the Humboldt Research Fellowship, Carl Friedrich von Siemens Research Fellowship, Japan Society for the Promotion of Science Visiting Fellowship, 2020 Best Paper Award for IEEE TRANSACTIONS ON INDUSTRIAL ELECTRONICS, and IEEE J. David Irwin Early Career Award.